Multipulse Operation and Limits of the Kerr-Lens Mode-Locking Stability

Vladimir L. Kalashnikov, Evgeni Sorokin, and Irina T. Sorokina

***Abstract*—Numerical analysis in combination with the experimental data for Cr^{2+}:ZnSe as well as Ti:sapphire lasers reveal the following main mechanisms of multiple-pulse generation for the Kerr-lens mode-locked solid-state lasers: 1) continuum amplification due to a spectral loss growth for ultrashort or chirped pulses and 2) a bounded perturbation rise for high-energy pulses. The role of such laser parameters as gain saturation and relaxation, saturable and unsaturable loss, self-phase modulation, Kerr-lensing, and pump intensity is analyzed. This analysis provides basic directions for single-pulse stability enhancement and for multiple-pulse generation control.**

***Index Terms*—Kerr-lens mode locking, multiple-pulse generation, ultrashort-pulse stability.**

I. Introduction

ULTRASHORT-PULSE laser oscillators demonstrate a tendency toward destabilization and pulse splitting when the pulse duration approaches minimal values (see, for example, [1]). As the net group-delay dispersion (GDD) in the resonator approaches zero, a nonregular pulsing or a stable multiple pulse generation may occur. Both the unstable as well as stable multipulse oscillation can be generally considered as the obstacle for pulse shortening. At the same time, it is possible to use pulse splitting for an additional duration decrease as well as for an increase of the laser repetition rate. The analysis of this phenomenon is not straightforward because the ultrashort-pulse laser is a complex system with different interacting nonlinearities.

At the moment, the following mechanisms for multipulse operation have been considered: the appearance of negative feedback due to the growth of the pulse chirp [2], the growth of the radiation scattering accompanying the decrease of the soliton period [1], the contribution of the higher order dispersions to laser dynamics [3], the growth of the laser continuum owing to the positive net gain of the background radiation outside the pulse [4], and the dynamical gain saturation and recovery [5]. Multipulse operation can also be considered as a result of the higher order soliton dissociation [6].

In the framework of the soliton approach [7], [8], it was shown that the multipulse oscillation can be caused by the formation of the bounded multisoliton complexes in resonators with both negative and positive net-GDD. The self-interaction of such bounded soliton-like complexes is governed by the relative phase of the constituent pulses [9]. The presence of the continuous local (i.e., through the pulse wings) interaction between the pulses distinguishes such bounded soliton-like complexes from the regimes created as a result of the repetition-rate multiplication due to the change of the gain and loss saturation balance in the system [10]–[12]. One should also distinguish the stable multipulse operation from the generation of the double pulses colliding in an active medium [13]–[16]. It should be noted that the transition to multipulse operation is not the sole scenario of the stability loss in the continuous-wave (CW) mode-locked solid-state lasers: the automodulational instability can produce regular as well as nonregular oscillations of the single pulse or the so-called picosecond collapse with the abrupt transition from the femtosecond to the picosecond generation [17], [18].

The stable multipulse operation in the negative GDD region was experimentally observed in Ti:sapphire [1], [19]–[21], Cr:LiSGaF [22] and Yb:KYW [23] Kerr-lens mode-locked lasers as well as in Nd:glass [24], Ti:sapphire [4], and Cr^{4+}:YAG [25] lasers mode locked by a semiconductor saturable absorber mirror. In [26], the tendency toward multipulse generation was reported for the positive-GDD regime in the Cr^{2+}:ZnSe laser with passive mode locking initiated by acousto-optical modulation.

The latter medium, allowing diode pumping and possessing excellent lasing characteristics [27], [28], is of interest as a tunable ultrashort pulsed mid-infrared (IR) source. At this moment, a variety of generation regimes have been demonstrated: the efficient pulsed [29] and CW [30], diode-pumped operation [31], active mode locking [32], and the active modulator-assisted passive mode locking [26]. Above all, Cr^{2+}:ZnSe is of interest as the model object for the study of multiple-pulse operation. This interest is explained by the combination of unique characteristics: very large nonlinear index of refraction [33] as well as emission and absorption cross sections. As it will be shown later on, these factors play a crucial role in pulse destabilization and transition to multiple-pulse operation.

In order to explain the variety of the observed multipulse regimes one needs to have a basic understanding of the nature of multiple-pulse generation in Kerr-lens mode-locked lasers. Our model takes into account the strong saturation of the Kerr-lens induced fast absorber, the gain saturation and recovery dynamics, the GDD and the self-phase modulation, making it valid for the different femto- and picosecond Kerr-lens mode-locked lasers and sufficiently simple to obtain the physically significant conclusions.

Our analysis reveal the existence of the two basic mechanisms causing multiple-pulse operation: the background amplification due to the gain saturation decrease and the increase of

Manuscript received March 18, 2002; revised October 21, 2002. This work was supported by the Austrian Science Fund (FWF) under Projects M688, M611, T64, and 14704-TPH, and by ISTC Project B631.

The authors are with the Photonics Institute, Technical University of Vienna, A-1040 Vienna, Austria (e-mail: vladimir.kalashnikov@tuwien.ac.at).

Digital Object Identifier 10.1109/JQE.2002.807204

the "bounded" perturbation in the presence of the strong saturation of the fast absorber. The basic laser factors defining the pulse stability were found to be the gain and loss saturation in combination with the spectral loss. As will be demonstrated, the inter-pulse interaction is strong enough to produce the correlations of the inter-pulse distances and phases, which are governed by the GDD and the fast absorber parameters. The statistical and multistable properties of the bounded multiple-pulse complexes will be considered as well. Finally, the limits of the single-pulse operation and the methods of the stability enhancement will be analyzed.

II. Model and Parameters of Simulation

Throughout this paper, we shall consider only the stable multiple pulses localized within the time window, which is much shorter than the cavity round-trip period. The period and repetition-rate multiplications as well as automodulational regimes will not be considered. We also assume that the laser mode is close to TEM_{00}. This allows the use of a one-dimensional propagation model and the parabolic approximation for self-focusing.

A. Model

The main challenge in the simulation of the Kerr-lens mode-locked lasers is a formulation of the model, which would adequately describe the laser dynamics and at the same time would not be too complicated to remain physically meaningful. The soliton approach, which fulfills the latter requirement, does not take into account the strong nonlinear behavior of the real-world femtosecond solid-state lasers. Therefore, we make use of the relatively simple, but sufficiently general numerical model, first presented in [34].

The split-step scheme for the simulations of the slowly varying field amplitude $a(t)$ evolution can be represented as

$$a_I(t) = a_{in}(t)\exp\left(-i\beta\left|a_{in}(t)\right|^2\right) \tag{1}$$

$$a_{II}(t) = a_I(t)\exp\left(-\frac{\gamma}{1+\sigma\left|a_I(t)\right|^2}\right) \tag{2}$$

$$a_{III}(t) = \frac{1}{2\pi}\iint_{-\infty}^{\infty} a_{II}(t')\exp\left(-t_f^2(\omega-\omega_0)^2 - i\omega(t-t')\right)dt'd\omega \tag{3}$$

$$a_{IV}(t) = a_{III}(t)\exp(\alpha-\rho) \tag{4}$$

$$a_{\mathrm{out}}(t) = \frac{1}{2\pi}\iint_{-\infty}^{\infty} a_{IV}(t')\exp\left(-iD(\omega-\omega_0)^2 - i\omega(t-t')\right)dt'd\omega \tag{5}$$

where the different steps within the full cavity round trip describe:

1) the self-phase modulation action (1), where $|a|^2$ is the field intensity, $\beta = 2\pi n_2 x/\lambda n$ (here, n_2 and n are the nonlinear and linear refraction indices, respectively, x is the double length of the active medium, and λ is the central oscillation wavelength);
2) the Kerr-lens induced fast saturable absorber action defining the self-amplitude modulation of the field, γ is the modulation depth, σ is the inverse intensity of the loss saturation (2); note that consideration of the strong modulation is necessary in our case owing to the low critical self-focusing power in ZnSe, which is only $\sim$0.2 MW [26] as a result of the large value of n_2;
3) the spectral filter action with the inverse bandwidth t_f, which coincides with the gain bandwidth, ω_0 is the field carrier frequency coinciding with the minimum of the spectral loss (3);
4) the homogeneously saturated gain and the output loss action with coefficients α and ρ, respectively (4);
5) the net-GDD action with the dispersion coefficient $D = d^2\phi/d\omega^2|_{\omega=\omega_0}$ where $\phi(\omega)$ is the linear phase retardation of the field (5). The full round trip results from setting $a_{\mathrm{in}}(t) = a_{\mathrm{out}}(t)$.

In practice, when the field change over the round trip is small (this is valid in our case), the scheme represents the distributed dynamical equation of the Ginzburg–Landau type in the presence of an arbitrarily strong loss saturation

$$\frac{\partial a(z,t)}{\partial z} = \left[\alpha-\rho-\frac{\gamma}{1+\sigma\left|a(z,t)\right|^2} + (t_f^2+iD)\frac{\partial^2}{\partial t^2} - i\beta\left|a(z,t)\right|^2\right]a(z,t) \tag{6}$$

where z is the formal longitudinal coordinate (the cavity round-trip number).

The scheme (1)–(5) or, equally, (6), has to be supplemented with an equation for the gain coefficient evolution, which for the quasi-two level amplification scheme has the following form:

$$\frac{d\alpha(t)}{dt} = \frac{I_i\sigma_a}{h\nu_a}\left(\alpha_{\max}-\alpha(t)\right) - \frac{\sigma_g\left|a(z,t)\right|^2\alpha(t)}{h\nu} - \frac{\alpha(t)}{T_r} \tag{7}$$

where I_p is the pump intensity, ν_a and ν are the pump and the lasing field frequencies, respectively, $\alpha_{\max}$ is the maximal gain for the full population inversion, σ_a and σ_g are the absorption and the gain cross sections, respectively, T_r is the gain relaxation time. When the pulse is much shorter than the cavity round-trip period T_{cav}, which is obviously the case, and the dynamical gain saturation is negligible (i.e., there is no time dependence of α on the scale of the pulse duration), which is correct for the sub-picosecond solid-state lasers, (7) can be easily integrated to eliminate the time dependence

$$\frac{d\alpha(z)}{dz} = P\left(\alpha_{\max}-\alpha(z)\right) - \frac{E}{E_x}\alpha(z) - \frac{T_{\mathrm{cav}}}{T_r}\alpha(z) \tag{8}$$

where $P = (I_p\sigma_a/h\nu_a)T_{\mathrm{cav}}$ is the dimensionless pump intensity, E is the pulse energy flux, and $E_s = h\nu/\sigma_g$ is the gain saturation energy flux.

The integration of (8) over z yields [17]

$$\alpha(z) = \alpha(z-1)\exp\left(-\frac{E}{E_s}-\frac{T_{\mathrm{cav}}}{T_r}-P\right) + \frac{\alpha_{\max}P}{\left(P+\frac{E}{E_s}+\frac{T_{\mathrm{cav}}}{T_r}\right)}\left[1-\exp\left(-\frac{T_{\mathrm{cav}}}{T_r}-P\right)\right]. \tag{9}$$

It is convenient to use dimensionless quantities in the calculations and we shall normalize the time to t_f and the field intensities to β^{-1}. Then, the pulse energy flux is normalized to t_f/β,

TABLE I
MATERIAL PARAMETERS OF Cr:ZnSe AND Ti:SAPPHIRE ACTIVE MEDIA

	T_r	λ	$\Delta\lambda$	n_2	n	σ_g	σ_a	λ_a
	μs	μm	nm	cm^2/PW		10^{-20} cm^2	10^{-20} cm^2	μm
Cr^{2+}:ZnSe	6	2.5	800	16	2.45	80	37	1.75
Ti^{2+}:Al_2O_3	3	0.8	200	0.3	1.76	30	20	0.488

TABLE II
EXPERIMENTAL AND MODEL PARAMETERS
(FOR DEFINITIONS, SEE SECTION II-A)

	x	w_0	T_{cav}	α_{max}	β	t_f	ϵ	P_{max}
	cm	μm	ns		cm^2/TW	fs		
Cr^{2+}:ZnSe	0.6	60	10	5.28	95	12.5	1.3×10^{-3}	1.6×10^{-4}
Ti^{2+}:Al_2O_3	1.5	14	12.3	0.33	21	2.5	1.46×10^{-4}	1.44×10^{-3}

resulting in the expression for the dimensionless inverse saturation energy flux $\epsilon = \sigma_g t_f/(h\nu\beta)$. This parameter plays a crucial role in our model since it describes the contribution of the gain saturation in the lasing dynamics in comparison to the contribution of the self-phase modulation. Other key parameters are P, which is the pump energy stored during the cavity period (in the units of absorption saturation energy), and the dimensionless parameter σ, which describes the strength of the self-amplitude modulation relative to the self-phase modulation. With this normalization, the field intensity $|a(t)|^2$ has the physical meaning of the dimensionless $\Phi(t)/\Phi_{\rm crit}$ ratio, where $\Phi(t)$ is the instantaneous power in the laser beam and $\Phi_{\rm crit} = 1.83\lambda^2/(4\pi n n_2)$ [33] is the critical power of self-focusing.

In the present form, the model is valid not only for the description of the Kerr-lens mode-locked solid-state lasers but also for other laser systems with fast saturable absorbers, such as the additive-pulse and self-polarization rotation mode-locked solid-state and fiber lasers. However, we have to note that in such schemes the strong loss saturation can turn to self-darkening, which produces the passive negative feedback and influences the pulse stability [35]. This effect cannot be described by (6), and the results of this paper can be applied to the additive-pulse and self-polarization rotation mode-locked systems only as a weak nonlinear approximation.

B. Parameters of the Model

In the numerical calculations, we assume a generic setup for a Kerr-lens mode-locked laser to employ a longitudinally pumped active medium, an arbitrary dispersion-compensating scheme, which together with the active medium provides the flat second-order dispersion, and an instantaneous n_2-based self-amplitude modulation mechanism.

This generic scheme is suitable to model practically all the published experimental studies of multipulsing in Kerr-lens mode-locked lasers in different active media [1], [13], [14], [19], [20], [22], [23], [26]. While our main interest stays with the case of the Cr:ZnSe laser [26], we also consider the Kerr-lens mode-locked Ti:Sapphire laser to verify our model. For the latter, we take the well-documented experiment in [13] for modeling. It is also important that for both experiments the setup parameters are available in every detail.

Table I summarizes the relevant material parameters of Cr:ZnSe and Ti:Sapphire, intrinsic to the chosen materials. In Table II, x, w_0, $T_{\rm cav}$, and $\alpha_{\rm max}$ represent the experimental parameters, which are used to obtain the modeling parameters β, t_f, ϵ, and $P_{\rm max}$. Intensities are calculated using the expression $\pi w_0^2 n$ for the mode area inside the active medium, taking into account the astigmatism of the Brewster-oriented crystal.

In the simulations, we consider the parameters in Table II as fixed, and P, ρ, GDD, γ, and σ as varying. In the experiment, this corresponds to the pump power adjustment, the exchange of the output coupler, the variation of the distance between the prisms and of their insertion, the slit width adjustment, and the stability zone and the lateral crystal position scans, respectively. If the Kerr-lens mode locking is based on the so-called soft aperture, then the γ and σ parameters are simultaneously changed by scanning across the stability zone, and the adjustment of the crystal position and the pump focusing lens.

The simulations are performed at the grid with 2^{13} points (102-ps time window) over 6×10^4 transits corresponding to 0.6 ms of the real time, which guarantees the convergence to the steady-state or, physically, the mode-locking self-start. The solutions with deviations of the peak intensity within 1% during the last 5000 transits are considered as steady state. The small intensity single spike is chosen as the initial condition for *ab initio* simulations. To make sure that the results are independent from the time window and step size, we performed cross-check simulations on the grid with 2^{19} points (6.6-ns time window, comparable to $\rm T_{cav}$) and on the grid with a time step equal to $t_f/2\sqrt{ln2}$.

III. MULTIPLE-PULSE OPERATION

In this section, we describe the characteristic features of multipulse operation in the regions of negative and positive GDD, the influence of the self-amplitude modulation strength, and the typical parameters of the stable complexes of the bounded multipulse solutions. To check the adequacy of the model, we compare its predictions with the experimental results for the Cr:ZnSe laser (positive GDD) and the Ti:sapphire laser (negative GDD).

A. Negative GDD

First, let us consider the case $D < 0$, which assures the quasi-Schrödinger soliton formation. As was shown in [17] on the basis of the aberrationless approximation, the soliton-like pulse, i.e., the pulse with the sech-time profile and the negligible chirp, exists in the parameter range, which is wider than the soliton model prediction, and becomes unstable in the vicinity of $D = 0$ due to the automodulational instability.

The behavior of the pulsewidth in our case is presented in Fig. 1 in dependence on the GDD variation. Approaching zero GDD results in the generation of multiple pulses (up to 24 for given parameters, the example of the triple pulses is shown in Fig. 2, the intensity of filling corresponds to value of $\log|a(z,t)|^2$). In Fig. 1, we depict only parameters of the double and the triple pulses. The single-pulse shortening caused by decreasing $|D|$ transforms into the double-pulse generation, then the triple-pulse generation, etc. Each bifurcation is accompanied by the drastic pulsewidth increase. The characteristic feature is the multistable lasing in the region

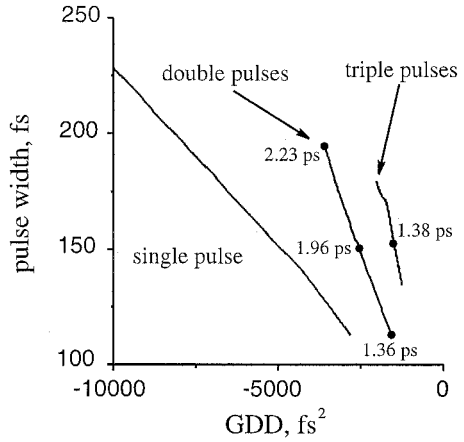

Fig. 1. Dependence of the pulsewidth on the GDD coefficient. Only single, double, and triple steady-state pulse characteristics are shown. Captions at points denote the inter-pulse distances. $P = 8 \times 10^{-5}$, $\sigma = 10$, $\epsilon = 1.3 \times 10^{-3}$, $\gamma = 0.02$, $\rho = 0.01$. Other parameters are mentioned in the text.

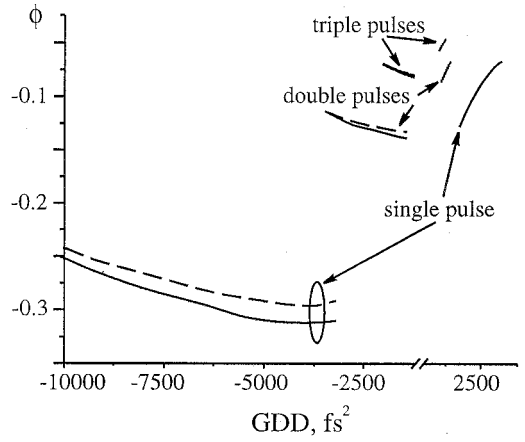

Fig. 3. Dependence of the single-transit phase retardation on the GDD coefficient. The negative GDD branches correspond to parameters of Fig. 1; the positive GDD branches correspond to $P = 1.6 \times 10^{4}$, $\sigma = 20$. The dashed curves show ϕ corresponding to Schrödinger soliton.

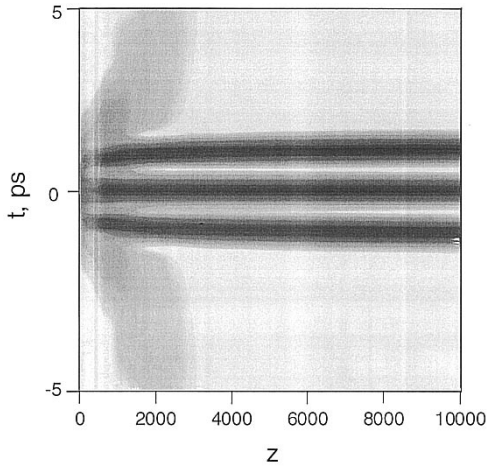

Fig. 2. Contour plot of the $|a(z,t)|^2$ logarithm for the stable triple-pulse operation. $P = 1.6 \times 10^{-4}$, $\sigma = 10$, $D = -2188 fs^2$. Other parameters correspond to Fig. 1. Darker regions correspond to higher intensity. z is the number of round trips.

of multiple-pulse generation: there exists a distinct hysteresis in the pulse parameters behavior (see Fig. 1). The pulse multiplication results in the strong instability in the vicinity of $D = 0$. Such behavior is not the noise or the CW operation, but multiple-pulse generation with strong coupling between the pulses and nonregular changes of their parameters.

To analyze the nature of the ultrashort-pulse destabilization, we shall consider the influence of the basic lasing factors: self-phase modulation, GDD, self-amplitude modulation due to the fast saturable absorber and the gain saturation, and the spectral filtering.

First, let us examine the nonlinear phase shift contribution. The solid curves in Fig. 3 show the phase-retardation ϕ at the steady-state pulse peak after the full cavity round trip. One can see that the phase shift is close to that for the Schrödinger soliton (dashed curves) and is small in comparison to π (especially for the lower intensity multipulse regimes). Hence, the self-phase modulation cannot produce the pulse spectrum fragmentation. Moreover, approaching the stability boundary does not cause any significant phase shift. As a result, there is no spectrum fragmentation in our case.

As an additional destabilizing factor, the dispersive perturbations in the laser system with self-phase modulation and negative net-GDD give rise to the spectral sidebands [1], [37], [38]. Their position in the absence of the higher order dispersion can be found from the condition $k_d = k_s \pm k_p$, where $k_d = D(\omega_{\rm sb} - \omega_0)^2$, $k_s = 2D/t_s^2$, and $k_p = 2\pi j$ are the normalized to inverse cavity length wave numbers of the dispersive wave, solitary wave, and periodic perturbation, respectively, $\omega_{\rm sb}$ is the sideband frequency, t_s is the width of the soliton-like pulse with the shape $\mathrm{sech}(t/t_s)$, and j is an integer. When $t_s^2 \gg |D|$, we have $\omega_{\rm sb} - \omega_0 \approx \pm\sqrt{2\pi j/|D|}$. Our simulations show that the spectral loss for the sidebands is too large in our case. Thus, the sideband generation does not contribute to the ultrashort-pulse destabilization for the given parameters. This prevents the scattering radiation growth [1] and illustrates the validity of the distributed model in our case.

Thus, we see that, in our case, neither the self-phase modulation-induced spectral fragmentation nor the sidebands generation caused by the dispersion perturbations produce multiple-pulse operation. However, the former mechanism can cause the chaotical behavior for $|D| \to 0$, where the abrupt nonlinear transformation due to self-phase modulation is not compensated by GDD. The latter mechanism, i.e., the sideband generation, can significantly influence the lasing due to the dispersion wave amplification when the pulsewidth approaches $\sqrt{|D|}$.

The transition to multiple-pulse generation cannot be comprehended without taking into account the dissipative laser factors, such as the spectral filtering and the saturable, linear, and spectral losses. Fig. 4 shows the dependencies of the absorber loss saturated by the pulse peak intensity and the spectral loss for the soliton-like pulse on GDD. One can see that the absorber is saturated (solid curves) and almost does not contribute to lasing. At the same time, approaching zero GDD leads to the shortening of the pulsewidth and broadening of the spectrum. This produces the pronounced spectral loss growth (dashed curves). Alternatively, for the comparatively large pulse durations caused, for example, by the large $|D|$, the essential spectral broadening

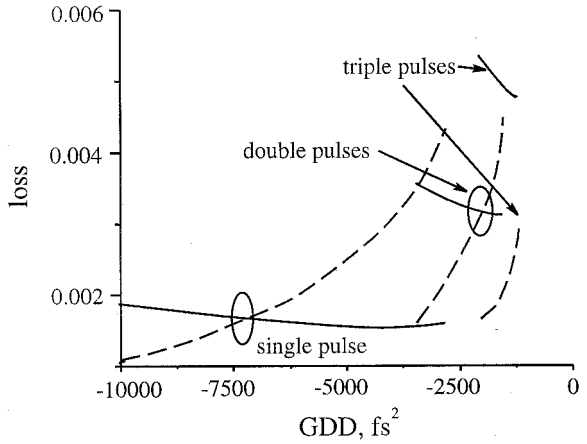

Fig. 4. Dependence of the saturated absorber loss $\gamma/(1+\sigma|a_{\max}|^2)$ (solid) and spectral loss (dashed) on the GDD coefficient for the parameters of Fig. 1. $|a_{\max}|^2$ is the steady-state pulse peak intensity.

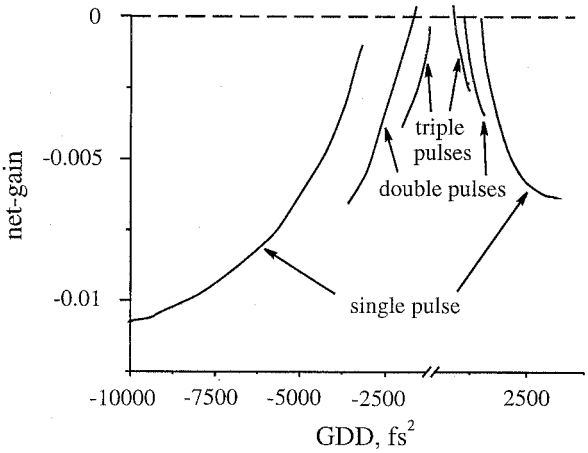

Fig. 5. Dependence of the net-gain coefficient $\alpha - \rho - \gamma$ on D for the parameters of Fig. 4.

results from the chirp growth in the vicinity of the stability boundary (but without spectral fragmentation). In both cases, the spectral loss decreases the pulse energy. Consequently, the gain saturation is reduced and the net gain $\alpha - \rho - \gamma$ increases and becomes positive (Fig. 5). This causes the background amplification on the pulse wings resulting in multiple-pulse generation (the analysis of the stability loss in the case of $\sigma\gamma \ll 1$ is given in [39]). The rise of the background with the subsequent multiple pulses appearance is clearly visible in Fig. 2.

B. Positive GDD

A very interesting property of the system is the stable multipulse generation in the region of the positive GDD (Section III-E). This regime excludes the Schrödinger soliton formation. The pulsewidth is shown in Fig. 6 in the dependence on GDD. The transition to multiple-pulse generation, as a result of $D \to 0$, has the hysteresis character and allows reducing the ultrashort-pulse durations essentially. In Fig. 6, only double- and triple-pulse regimes are presented, but in the vicinity of zero GDD, there may exist an even larger number of pulses (up to 28 in our case), which have durations reduced down to 300 fs. There exist certain parameter sets when the pulses fill

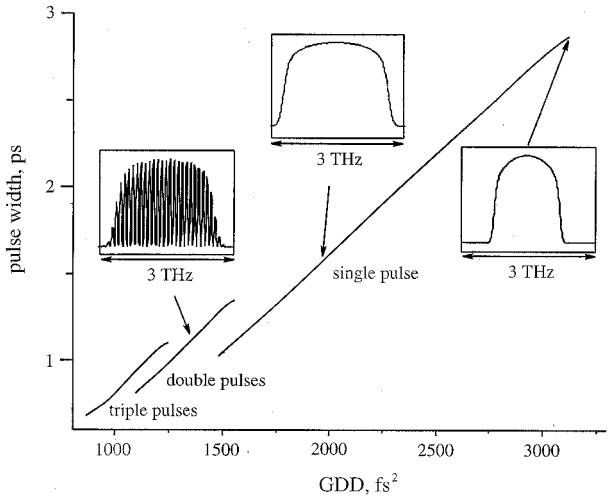

Fig. 6. Dependence of the pulsewidth on the GDD coefficient (only single-, double-, and triple-pulses regimes are shown). $P = 1.6 \times 10^{-1}$, $\sigma = 20$. The insets show the pulse spectrum profiles (a.u. at vertical axes).

the whole simulation window. In the vicinity of zero GDD, the accuracy of the pulse characteristics is rather low, because our model does not take into account the higher order dispersion, which strongly contributes to the pulse dynamics in this case.

As it was in the case of the negative net-GDD, the round-trip phase retardation is not sufficient for the pulse spectrum fragmentation, although it has a stronger dependance on D (Fig. 3).

Our analysis demonstrates that the signatures of the transition to multipulse generation are similar to those for the case of the negative GDD:

1) the approach to zero GDD increases the pulse intensity due to the dispersion spreading decrease;
2) as a result, the fast absorber saturates (although less than in the negative GDD domain);
3) the gain saturation decreases;
4) multipulse generation appears due to the background amplification [the net gain becomes positive (Fig. 5)].

The decrease of the gain saturation results from the pulse energy decrease. The source of the energy decrease for the positive GDD is the spectrum broadening (see inserts in Fig. 6) due to an increase of the self-phase modulation for small D, which is caused by the pulse intensity growth in the vicinity of zero GDD.

Thus, we have identified the actual pulse breakup condition which is the same for positive and negative GDD regimes: crossing of the net gain $\alpha - \rho - \gamma$ of the zero line, caused by the spectral widening of the pulse at decreasing GDD.

C. Variation of the Self-Amplitude Modulation

The variation of the σ parameter, which corresponds to the change of the loss saturation intensity, is the common way to adjust the mode-locking efficiency in a typical Kerr-lens mode locking setup. For example, the growth of σ, corresponding to the saturation intensity decrease, can be achieved by setting the laser operating point closer to the edge of the cavity stability range [40]. As was shown in [2] and [40], the typical normalized to the self-phase modulation coefficient values of σ lie in the range of $1 \div 100$ for the four-mirror Ti:sapphire laser.

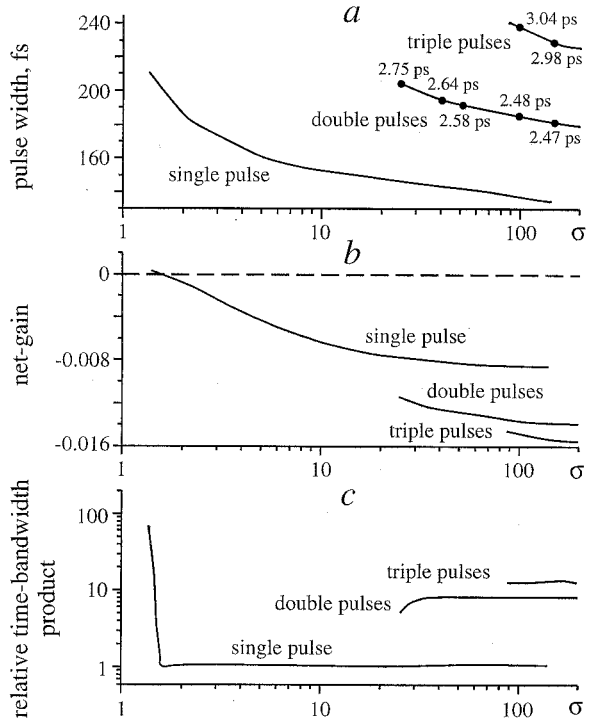

Fig. 7. (a) Pulsewidth. (b) Net-gain coefficient outside the pulse. (c) Time-bandwidth product related to the one for the Schrödinger soliton for the single, double, and triple pulses versus σ. Captions at points denote the inter-pulse distances. $P = 8 \times 10^{-5}$, $D = -5000 fs^2$.

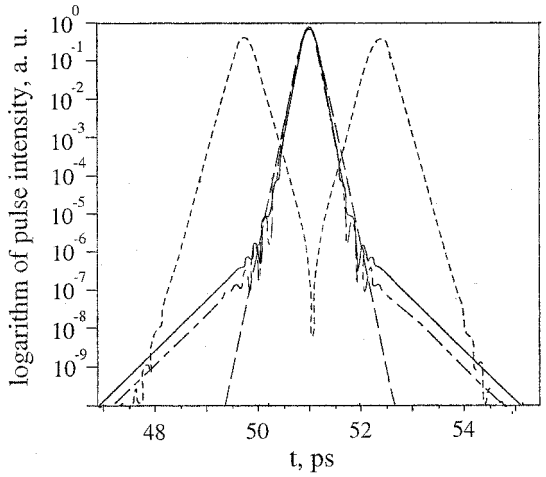

Fig. 8. Logarithm of the pulse intensity for $\sigma = 38$ (solid), 30 (dash-dotted), and 39 (dotted). Dashed curve correspond to the soliton profile.

As Fig. 7(a) shows, the increase of σ shortens the ultrashort pulse. Such shortening is accompanied by the growth of the phase retardation, the pulse energy, and the intensity due to the saturation of the fast absorber. The energy rise decreases the net gain outside the pulse due to the gain saturation [Fig. 7(b)]. It should be noted that for the given parameters the single pulse is almost chirp-free for the increasing σ [Fig. 7(c)].

The most interesting phenomenon caused by the σ change is the existence of the mechanism of ultrashort-pulse destabilization, which differs from the one considered above. We can see from Fig. 7 that there exists the minimum and the maximum of σ protected from the pulse destabilization. The small σ does not allow the fast absorber saturation. The absorber loss remains high, the pulse energy does not grow, and as a consequence, the gain cannot saturate. Hence, the net gain becomes positive. This results in the pulse destabilization due to the background radiation growth (Section III-A).

The existence of the maximum σ providing the pulse stabilization is less trivial. As we can see from the figure, the transition to multiple-pulse generation due to the increasing σ is not accompanied by the sign change of the net-gain coefficient. In this case, there is no satellite growing outside the pulse: the pulse dissociates by itself. In the framework of the linear perturbation analysis (weak nonlinear limit $\sigma\gamma \ll 1$), the satellite growth can be described by the excitation of the perturbation modes with continuous spectrum, while the pulse dissociation corresponds to the discrete spectrum of the perturbations. The loss saturation forms the *potential well*, which can contain the nondecaying bounded "states" corresponding to the perturbations. This property is enhanced by the potential deepening and widening, i.e., with the pulse energy growth. (For examples of the slow saturable absorber case, see [41] and [42].) The numerical analysis outside the weak nonlinear approximation also demonstrates the pulse destabilization due to the self-amplitude modulation growth in the absence of the background amplification [43]. The wings of such perturbations are visible in Fig. 8. Here, the solid and dash-dotted curves show the field intensity in the vicinity of the stability threshold and far from it, respectively. The dashed line corresponds to the profile of the sech pulse. The slowly decaying exponential wings corresponds to the "bounded" perturbations, which increase as a result of the approach to the stability boundary (transition from the dash-dotted to the solid curve). As the increase of the pulse intensity saturates the fast absorber, its discrimination strength decreases [13], thus favoring the perturbation growth and the pulse dissociation (dotted curve). The described picture agrees qualitatively with the analytical analysis presented in [45], where the complex amplitude of the perturbation is proportional to the pulse energy and the parameter of the saturation of the self-amplitude modulation. The profile of this perturbation is close to the dotted curve in Fig. 8 [45].

We have to note also the existence of the strong multistability as a result of the σ increase (Fig. 7). The region of the single and double (and even triple) pulses coexistence is wide and becomes apparent as a result of the variation of the initial field in the simulations. If we start from the arbitrary initial (regular) field, the probability of multiple-pulse generation is increased by the σ increase.

D. Bounded Multiple Pulses

As has been found, multipulse generation can be caused by the formation of the bounded soliton-like complexes with strong correlation between components (see, for example, [4] and [7]–[9]). The stability of the spectrum modulation in the experiment suggests nearly constant inter-pulse distance and phase difference.

The presence of the different mechanisms of the ultrashort-pulse destabilization somewhat complicates the picture. The number of the pulses in the bounded soliton-like complex does not depend on the initial field only in the regions, where

there is no multistability. Outside these regions, the number of pulses, their intensity and durations depend on the initial conditions.

The inter-pulse distance is more sensitive to the initial conditions. The multiple pulses formed by the continuum amplification have, as a rule, random distances because the pulse can rise at the arbitrary moment within the cavity period. However, the inter-pulse distance approaches the constant for the regular initial signal due to an interaction of the pulses arising from the common seed.

In the case of multiple-pulse generation caused by the bounded perturbation growth, the pulses evolve through the dissociation of the initial single pulse. Because the pulses stay close coupled all the time, interaction between the pulses plays a major role and the inter-pulse distance becomes less dependent on the initial conditions.

In practice, the presence of the mode-locking startup assistance (for example, due to the acousto-optical modulator [26]) will regularize the initial field and produce the repeatability of the inter-pulse distances. However, the dissociation of the bounded multiple-pulse complex always has the nonzero probability if only a fast saturable absorber is involved.

The interaction between the pulses in the bounded soliton-like complex can result from the soliton interaction mechanism and from the binding potential formed by dissipative factors. The mechanism of the Schrödinger solitons interaction was analyzed in the framework of the inverse-scattering formalism [46]. It was found that the motion of the soliton pair can be described as being influenced by the effective force, which depends on their relative phase φ, amplitude, and distance δ. In the specific case of $\varphi = 0$ and the equal amplitude of the interacting solitons, such interaction causes the periodic collapse of the bounded multiple-pulse complex with the period $z = [\pi \sinh(2\delta_0)\cosh(\delta_0)]/[2\delta_0 + \sinh(2\delta_0)]$ [47], where δ_0 is the initial inter-soliton distance normalized to the soliton duration and z is normalized to the dispersion length. If we take the parameters of Fig. 1, this formula gives a time of 2×10^6 cavity round trips as the double pulses collapse period. It is obvious that it is too small to explain the observed steady-state behavior of multiple-pulse complexes, which are interferometrically stable over seconds in the experiment. Hence, the soliton mechanism cannot be considered as the single and main source of the pulse interaction. First, this mechanism does not describe the situation of the positive GDD and second, the contribution of the spectral dissipation reduces the interaction of the Schrödinger solitons [9], [48], [49].

As was found in [7], the perturbation of the nonlinear Schrödinger equation by the linear and nonlinear loss terms and by the spectral filtering produces the oscillating soliton wings. The overlapping of these wings forms the soliton interaction potential, which has a minimum. In fact, the interaction through the oscillating pulse wings is suppressed in our case due to the damping of the sideband generation (Fig. 8, [50]). Nevertheless, we suppose that the spectral loss [4] and the fast absorber saturation may contribute to the interaction of the pulses.

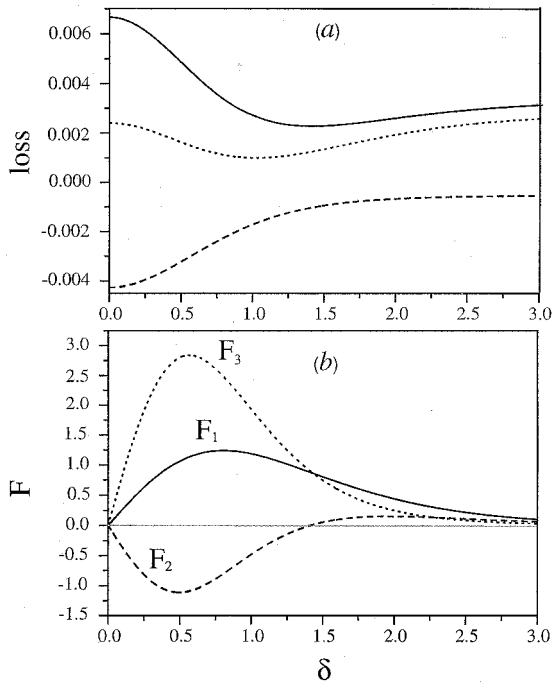

Fig. 9. (a) Energy loss for the spectral filter (solid), the saturable absorber (dashed), and their common action (dotted). (b) Functions F_1 (solid), F_2 (dashed), and F_3 (dotted). $a_0 = 0.1$, $\sigma = 1$, $\varphi = 0$, $t_p = 12\, t_f$, $\gamma = 0.02$. Inter-soliton half-distance δ is normalized to the pulse duration t_p.

Let us consider (6) from this point of view. There is the method to analyze the pulse interaction, which is based on the study of the conserved momenta of (6) [8]

$$\int_{-\infty}^{\infty} |a|^2 dt, \quad \mathrm{Im} \int_{-\infty}^{\infty} a \frac{\partial a^*}{\partial t} dt.$$

Multiplying (6) by a^*, adding the complex conjugate, and integrating over t results in

$$\frac{1}{E}\frac{dE}{dz} = 2(\alpha - \rho - \gamma) - \frac{2t_f^2}{E}\int_{-\infty}^{\infty}\left|\frac{\partial a}{\partial t}\right|^2 dt + \frac{2\gamma\sigma}{E}\int_{-\infty}^{\infty}\frac{|a|^4}{1+\sigma|a|^2}dt \quad (10)$$

which is the energy balance equation for the laser field.

Let us consider as the simplest example a superposition of two pulses

$$a(t) = a_0\{\mathrm{sech}(t-\delta) + \mathrm{sech}(t+\delta)\exp(i\varphi)\}$$

where δ is the half-distance and t and δ are normalized to the pulse duration).

It is obvious that the interference between the pulses alters the energy "transmission" increment [right-hand side of (10)]. Fig. 9(a) shows the energy loss due to the spectral filtering (solid curve), the absorber saturation (dashed curve), and their common action (dotted curve) in the dependence on δ $(\varphi = 0)$. One can see that there exists the minimum of spectral loss for $\varphi = 0$ and $\delta \approx 1$. The appearance of this minimum is demonstrated in Fig. 10. The merged pulses suffer the larger spectral loss as a result of the widest spectrum (solid curve). The

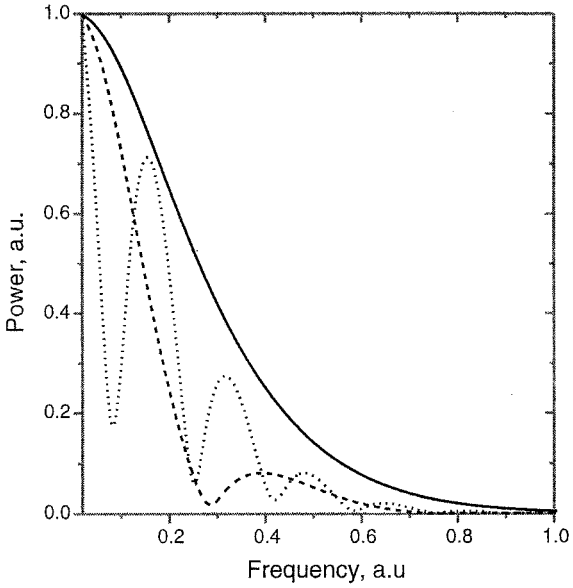

Fig. 10. Spectrum of the double-pulse complex with $t_f = t_p/1.76$, $\delta = 0$ (solid line), and 0.6 (dashed line), 1.8 (dotted line). δ is normalized to t_p.

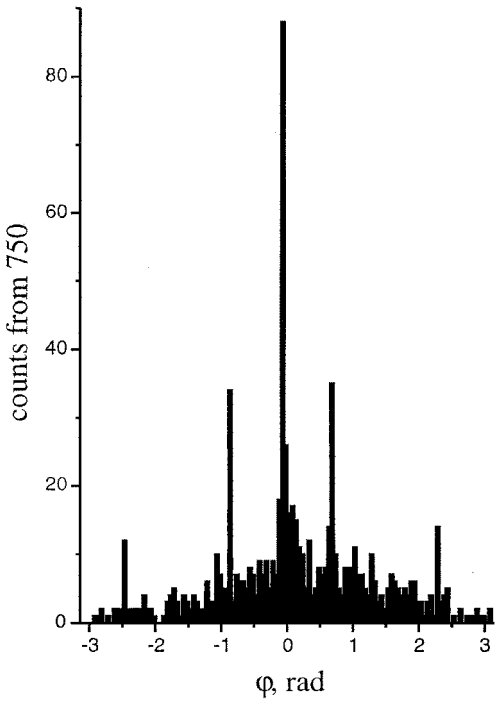

Fig. 11. Histogram of the phase differences accumulated for the different double- and triple-pulses regimes.

δ increase splits the spectrum and concentrates the energy in its central part (dashed curve). The spectral loss is minimum in this case. The further distance increase forms the more uniform modulation with the rise of the high-frequency part (dotted curve). As a result, the spectral loss approaches that of the single pulse. The spectral loss decrease produced by this mechanism is larger for the shortest pulses. Hence, the region of its action extends for the distances $\sim 5 \div 8t_p$. The chirped pulses interact even more strongly.

The next obvious mechanism is the fast absorber saturation, which favors the pulses merging due to the stronger loss saturation for the overlapping pulses. In the calculation, we took into account only the first term in the expansion on $\sigma|a|^2$ in the last term of (10) (dashed curve in Fig. 9(a); this treatment is similar to that for the explanation of the colliding-pulses regime in [13], where the double-pulse generation resulted from the stronger Kerr lensing for the colliding pulses). The combination with the spectral filtering can lead to the "absorption" of the pulses into the "potential well" for the comparatively small a_0 and σ (dotted curve in Fig. 9(a). But the increase of the field amplitude and the saturation parameter lead to the pulse merging in the simplified model of (10) because the last term approaches the maximal value of 2γ as a result of the pulse amplitude or σ growth. Currently, it is not quite clear what mechanism prevents the pulses from collapsing. It is obvious, however, that the distance between the pulses is a result of the balance between the pulling force (the fast absorber saturation) and the as-yet unclear repulsion mechanism. The pulse intensity growth causes stronger saturation of the absorber and, therefore, increases the pulling force. This is illustrated by Fig. 7(a) and (1), where inter-pulse distance decreases with intensity growth caused by the σ increase and $D \to 0$, respectively.

Some additional aspects of the pulse interaction can be revealed by the consideration of the second momentum of (6), which describes the force acting on the pulse along the t axis

$$\mathrm{Im}\int_{-\infty}^{\infty} a\frac{\partial a^*}{\partial t}dt = 2a_0^2\sin(\varphi)\left((\alpha-\rho)F_1(\delta) + t_f^2F_2(\delta) - \gamma F_3(\delta,\varphi,\sigma a_0^2)\right) \quad (11)$$

where $F_1(\delta)$ and $F_2(\delta)$ are the functions of δ and describe the linear loss and gain action and the spectral filtering, respectively, and $F_3(\delta,\varphi,\sigma a_0^2)$ is the function of δ, φ, peak intensity a_0^2, and σ, and describes the fast absorber action. F_1, F_2, and F_3 have an analytical form, but the expressions are overcomplicated and not instructive. A typical case is illustrated by Fig. 9(b). Besides the trivial stationary points $\varphi = 0, \pm\pi$, there exists some inter-pulse distance causing zero interaction due to spectral filtering (intersection of $F_2(\delta)$ with zero line). As F_3 depends also on φ and σa_0^2, the right-hand side of (11) can vanish at values of φ which differ from 0, $\pm\pi$. Thus, the stable pulses can have various phase differences.

Our calculations demonstrate, that the phase difference changes in the process of the pulse evolution, in agreement with [4], [9]. The simulation also reveals the existence of the "attracting" set of φ values. The vicinity of these points is the most probable place for the pulse to stay, as demonstrated by the histogram in Fig. 11. This histogram was accumulated from 750 multiple-pulse regimes corresponding to the various system parameters as well as the various initial conditions. We suppose, that the existence of this attracting set explains the spectrum regularity, which is observed experimentally.

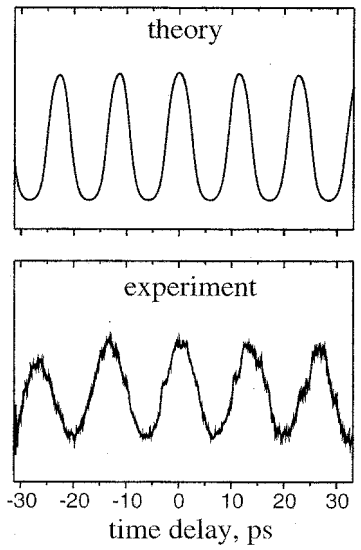

Fig. 12. Simulated and experimental autocorrelations of multiple-pulse Kerr-lens mode-locked Cr:ZnSe laser.

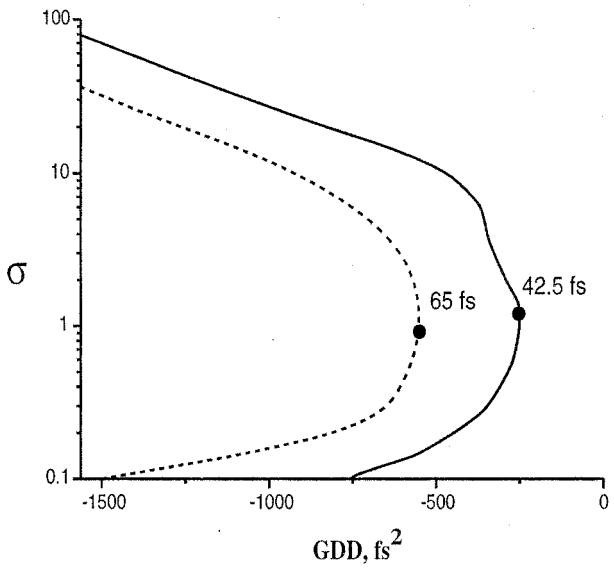

Fig. 13. Regions of pulse stability for Ti:sapphire laser. Solid and dashed lines represent the single-pulse stability boundary for $\gamma = 0.024$ and $\gamma = 0.015$, respectively.

It should be noted, that the unbounded multiple-pulse complexes can be stable over the whole simulation time. As the difference between the pulse intensities in the soliton-like complex, as a rule, is small enough, this causes the constant phase difference during the large time period. The last results in the experimentally observed regular spectra for the pulses with large and nonuniform δ.

E. Cr:ZnSe Laser (Positive GDD)

For modeling, we have chosen the experiment described in [26] with the following simulation parameters: $P = 2 \times 10^{-4}$ (corresponds to 1.5 W absorbed pump power at 1.61 μm), output coupling $\rho = 0.01$, and $GDD = 3500\text{fs}^2$ (material dispersion of the Cr:ZnSe crystal and acousto-optic modulator). As Kerr-lens mode locking mechanism was of the soft-aperture type, the exact value of the σ parameter is unknown. The level of saturable losses γ was estimated from the output power level to be up to two times higher than the losses due to the output coupler. In the simulation, the ranges of γ and σ are $0.01 \div 0.02$ and $5 \div 10$, respectively.

Within these ranges, the modeling predicts stable multipulsing with 2–28 pulses simultaneously present in the cavity. The typical pulse duration was 0.3–5 ps; distance between pulses was 1–15 ps. Fig. 12 compares the simulated autocorrelation trace (pulse duration 4.4 ps, pulse distance 11.3 ps) with the experimental autocorrelation signal [26] (pulse duration 4.5 ps, distance 13.5 ps). The result was obtained using $\gamma = 0.02$ and $\sigma = 10$ parameters, both within the expected range of parameters and demonstrates validity of the model in the positive GDD regime.

F. Ti:Sapphire Laser (Negative GDD)

The multipulsing behavior of this laser is well-documented (see, for example, [4], [13], [19] and [20]). We shall apply our model to the experiment from [13] inasmuch as in this study the stability of the single-pulse generation was the subject of the special investigation and comprehensive experimental data is available.

We choose the following simulation parameters: $P = 1.44 \times 10^{-3}$, corresponding to 2.5 W pump power at 488 nm with 28 μm Gaussian beam diameter; output coupling $\rho = 0.025$; $\gamma = 0.044, 0.024, 0.015$, corresponding to 1.5-, 2-, and 2.5-mm aperture diameters, respectively.

We obtained the following results of the simulations. For the maximum diffraction loss ($\gamma = 0.044$), both CW and ultrashort-pulse generation are suppressed as it took place in the experiment. The choice of the other two values of γ results in the stable single-pulse generation. The corresponding regions are shown in Fig. 13, where the curves, as usually, represent the boundaries of the single-pulse stability regions. $\gamma = 0.024$ is close to the optimal value of the modulation depth ([13, Fig. 1]). In this case, the single-pulse generation takes place in the widest region on our parametrical plane (solid curve). The minimal pulse duration is 42.5 fs, which is in good agreement with the experimental data ([13, Fig. 2]). The estimated experimental values of σ were $\approx 0.5 \div 0.7$, which are close to the optimal values in our simulations (Fig. 13) and are located on the lower stability boundary. The destabilization for these σ occurs when $D > -350 fs^2$. This quite agrees with the experimental data.

The decrease of γ produces the shortening of the single-pulse stability region (dashed curve in Fig. 13). In this case, as was found in [13], the single-pulse operation is suppressed by multipulsing or CW generation. As a result, the minimum pulse duration increases due to higher minimum $|D|$.

This comparison demonstrates that the model is in quantitative agreement with the experimental data for the Ti:sapphire laser and the considered pulse destabilization scenarios have a general character.

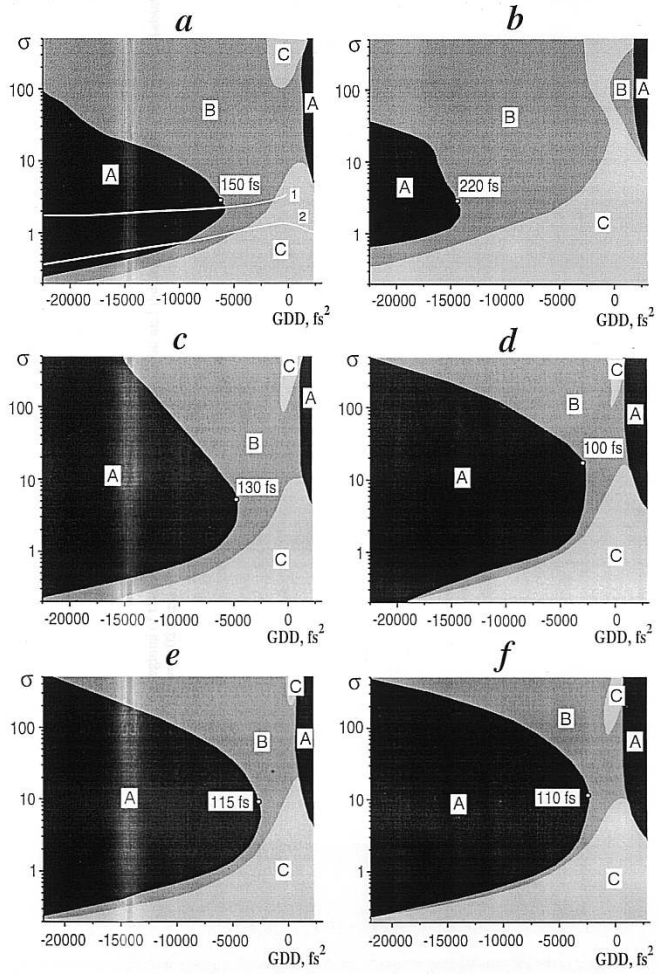

Fig. 14. Regions of pulse stability. The parameters are varied relative to (a). (b) γ decrease. (c) ρ increase. (d) ϵ increase. (e) Pump decrease. (f) T_r decrease. P=1.6 $\times$ 10^{-4} (a–d, f), 8 $\times$ 10^{-5} (e); $T_r = 6\,\mu$s (a–e), 3 (f); $\epsilon = 0.0013$ (a–c, e, f), 0.0026 (d); $\rho = 0.01$ (a, b, d - f), 0.02 (c); $\gamma = 0.02$ (a, c–f}), 0.01 (b). Regions marked A are the regions of the stable single-pulse generation, B are the regions of the stable multiple pulse operation, and C are the regions of the chaotical or CW lasing. Curve 1 shows the parameters providing the chirp-free pulse generation in the soliton model; curve 2 is the limit of the pulse stability from the soliton model.

IV. Limits of Ultrashort-Pulse Stability

As was shown in Section III, there exist two basic mechanisms of the ultrashort-pulse destabilization which cause stable multipulse operation, *viz.*, background amplification due to insufficient gain saturation by the pulse with reduced energy or excitation of the perturbation bounded within the high-energy ultrashort pulse. Hence, there may exist a certain range of parameters providing a stable ultrashort-pulse operation.

Fig. 14(a)–(f) demonstrates such regions on the parametric plane, *viz.*, the GDD and σ coefficients. Increase of σ corresponds to a shift toward the edge of the cavity stability region. The confined regions marked A correspond to the stable single-pulse operation (for negative as well as positive values of the GDD coefficient). The B regions depict the stable multipulse operation. Finally, the C regions are the domains of the unstable pulsed operation or the CW generation (on the lower boundaries of B). In Fig. 14, graph (a) is used as the reference and (b)–(f) are obtained by variation of only one of the parameters. In particular, (b) illustrates the decrease of the modulation depth γ, graph (c) the increase of the output loss ρ, graph (d) the increase of the ϵ parameter, graph (e) the decrease of the pump P, and graph (f) the decrease of the gain relaxation time T_r.

As we can see, there always exist certain upper and lower limits on σ for stable single-pulse operation. The lower boundary (small σ, i.e., the absorber is too "hard" to be saturated) is caused by the background amplification and can separate the single-pulse operation from the multiple pulses, as well as from CW lasing (for the positive and large negative GDD). The upper boundary (large σ, i.e., "soft" absorber with low saturation intensity) results from the destabilization due to the bounded perturbation growth. It should be noted, that as a result of the strong hysteresis, the upper stability boundary has a "fuzzy" character (Fig. 7).

A. Nature of the Stability Boundaries

The σ_{lower} decreases as a result of the $|D|$ increase. Such behavior can be obtained also on the basis of the soliton model. For example, in the weak-nonlinear limit, one can obtain the following condition of the background amplification [2]

$$\sigma \geq \frac{1-D\left(\sqrt{1+D^2}\right)}{\gamma\left[3\sqrt{1+D^2}-2D+2D^2(\sqrt{1+D^2}-D)\right]} \underset{|D|\to\infty}{\longrightarrow} \frac{1}{4\gamma|D|}$$

shown by curve 2 in Fig. 14. Here, we keep the normalization of σ and D to β and t_f^2, respectively. We have only qualitative agreement with the numerical results owing to the weak-nonlinear approximation and the simplified model of the gain behavior in the referenced model. However, even this simplified model agrees with numerical calculation for the lower stability threshold by the order of σ magnitude.

As can be seen from Fig. 14, the behavior of the lower stability boundary in the region of positive GDD agrees with our qualitative treatment as well. We have to stress that the destabilization in the framework of the soliton model takes place only for the chirped pulses, while it is not a necessary condition in the numerical model in the region of negative GDD. Curve 1 in Fig. 14 shows the location of the system parameters corresponding to the chirp-free sech pulse for the weak-nonlinear approximation (this is $\sigma = 1/(|D|\gamma)$ [17]; we keep the usual normalizations). The vicinity of the stability boundary to this curve causes the destabilization of the nearly chirp-free pulse.

The agreement with the soliton model results from the comparatively small loss saturation for small σ. The strong deviation from the weak-nonlinear model takes place for $|D| \to 0$, where the pulse intensities are sufficiently large for the strong loss saturation.

The referenced expression for σ_{lower} explains also the increase of the stability boundary as a result of the modulation depth decrease [see lower boundary of the A region for $D < 0$ in Fig. 14(b)] and the weak dependence of the lower stability boundary on other laser parameters, with the exception of ϵ for the large values of $|D|$ [Fig. 14(c), (e), (f)]. Formally, the dependence of σ_{lower} on γ is obvious in the weak-nonlinear approximation: the expansion of (6) on $|a|^2$ gives $\gamma\sigma$ as the self-amplitude modulation coefficient in the first order. The γ decrease

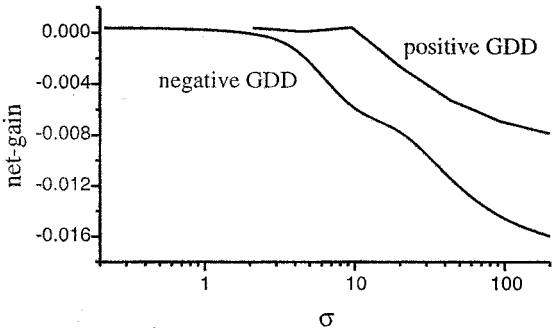

(a)

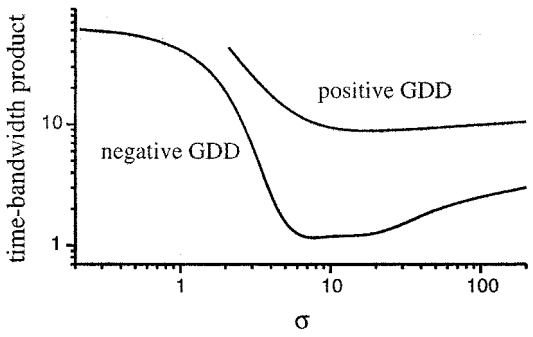

(b)

Fig. 15. (a) Net-gain and (b) time-bandwidth product related to the Schrödinger soliton one at the single-pulse stability boundary shown in Fig. 14(a).

reduces the contribution of the self-amplitude modulation, i.e., the difference between the pulse and background net gain, thus favoring the pulse destabilization.

The influence of the self-phase modulation on the pulse stability can be interpreted in the following way. Increasing β favors the pulse destabilization because the pulse energy decreases with growing spectral loss as a result of the pulse-spectrum expansion. Additionally, this spectral expansion reduces the gain saturation $\epsilon \propto 1/\beta$. This also leads to pulse destabilization by the background. The ϵ growth intensifies the gain saturation and so stabilizes the pulse against the background amplification [Fig. 14(d)]. Here, we do not consider the possible stabilization against automodulations produced by the self-phase modulation [17].

The contribution of the destabilization due to the bounded perturbation growth complicates the picture. Since the amplitude of such perturbation scales with the pulse energy [42], [44], the decrease of the pulse energy will result in the pulse stabilization against this instability. The pulse energy decreases for $|D| \rightarrow \infty$, but increases with σ. Hence, the σ_{upper} defining the pulse destabilization increases due to the $|D|$ increase (Fig. 14). For some $|D|_{\min}$, switching between destabilization mechanisms is possible (see the transition from the positive to the negative net gain and from the chirped to chirp-free pulses at the stability boundary presented in Fig. 15). Since the pulse duration decreases with $|D|$ decrease, such switching (if it takes place) confines the minimal duration of the ultrashort pulses (the minimal pulsewidths are shown by points in Fig. 14). It should be noted that destabilization due to the spectral loss can occur also due to the chirp growth. This is illustrated by Fig. 15(b), where the pulse spectral width at the stability boundary is shown to be as much as 50 times that of the bandwidth-limited pulse.

Thus, the existence of the minimal and maximal σ defining the pulse stability results from the two different mechanisms of the ultrashort pulse destabilization, *viz.*, the destabilization due to the continuum growth and pulse splitting due to the increase of the bounded perturbations. The twofold character of the destabilization complicates the laser optimization, as considered in the next section.

B. Pulse Stabilization

In this section, we summarize the ways to achieve the stable single-pulse operation in the system prone to multiple-pulse lasing. As the shortest pulsewidth for the fixed GDD is achieved by the σ growth, the main goal of the system's optimization is to enhance the stability against the bounded perturbations. The obvious way in this direction is the decrease of the intracavity energy. Such decrease can be undesirable for some systems (the high-power pulse sources, for example) and can degrade the self-start ability for the Kerr-lens mode-locked lasers. Moreover, this decrease can reduce the gain saturation and enhance the destabilization due to the background growth.

Let us describe the main approaches to the single-pulse stabilization.

1) The increase of the modulation depth, i.e., the γ parameter, expands the region of the single-pulse generation with subsequent pulse shortening and reduces the zone of unstable operation (transition from b to a in Fig. 14). It should be noted that such scenario decreases the self-starting ability, and may be a bad choice for many solid-state lasers. However, this way is acceptable for the Cr^{2+}:ZnSe laser due to its large values of n_2 and P (for given pump intensity I_p).
2) The increase of the linear loss ρ expands the stability region for the single-pulse operation. However, the pulse shortening that can be achieved in this way is comparatively small [compare Fig. 14(a) and Fig. 14(c)]. This is so because the background amplification is not suppressed in this case owing to the reduced gain saturation (pulse energy is lower in the case of higher ρ), so that there is only small improvement to the minimum GDD defining the minimal pulse duration.
3) The most appropriate choice is the increase of the ϵ parameter [Fig. 14(d) in comparison to Fig. 14(a)]. The increase of the gain saturation in comparison to the self-phase modulation contribution prevents both the background and bounded perturbation growth. Unfortunately, this parameter is constant for the given laser medium with fixed length x. Taking shorter active medium with the same $\alpha_{\max}$ enhances the stability. In this context, the Cr^{2+}:ZnSe is very attractive in comparison to other media due to the large value of ϵ. For example

$$\epsilon_{\text{Cr:ZnSe}} = 1.3 \times 10^{-3}$$
$$\epsilon_{\text{Cr:LiSAF}} = 6.9 \times 10^{-4}$$
$$\epsilon_{\text{Yb:KYW}} = 6.3 \times 10^{-4}$$
$$\epsilon_{\text{Ti:sap}} = 3.6 \times 10^{-4}.$$

The high value of n_2 for ZnSe is partially compensated by the large σ_g, λ, and n (see definition of ϵ in Section II).

4) Another approach is to decrease P by decreasing I_p or $T_{\rm cav}$ [Fig. 14(e) in comparison to Fig. 14(a)] or to decrease T_r [Fig. 14(f)]. Unfortunately, the advantage of Cr^{2+}:ZnSe consisting in its large absorption cross section turns into disadvantage: other parameters being equal, the larger σ_a and smaller ν_p result in the larger P. For example, for 1.5 W of the absorbed pump power at the center of the corresponding absorption lines and 100 μm diameter of the pumping beam, $P_{\rm Cr:ZnSe} = 5.9 \times 10^{-4}$, $P_{\rm Yb:KYW} = 6.3 \times 10^{-5}$, $P_{\rm Ti:sap} = 5.4 \times 10^{-5}$, and $P_{\rm Cr:LiSGaF} = 1.2 \times 10^{-5}$. The upper-laser level lifetime T_r is the material constant, and can be reduced (e.g., by heating or concentration quenching) only at the expense of higher laser threshold.

It should be noted that, according to Fig. 14, the pulse intensity decrease provided by the methods 2)–4) increases value of σ, at which the minimum pulse duration is achieved. This can demand a very thorough optimization of the laser design. Note also that the finger-like shape of the stability region for the small negative GDD providing the minimal pulse durations requires fine system optimization by the appropriate choice of σ. This feature is more critical for higher γ [compare Fig. 14(a) and (b)].

V. Conclusion

The numerical analysis taking into account the saturable gain, the spectral filtering due to the gain band profile, the net-group-delay dispersion, the self-phase modulation, and the fast loss saturation induced by the Kerr-lensing in the active medium allows the identification of the main sources of multiple-pulse generation in the Kerr-lens mode-locked solid-state lasers. As was shown, the nature of the single-pulse destabilization leading to multipulsing is defined by the interplay between the gain and loss saturation in the combination with spectral filtering.

The stable single-pulse operation in the negative as well as positive GDD regions is limited by the saturation parameter, so that for the fixed GDD there exist its lower and upper values confining the single-pulse stability region. The lower stability boundary corresponding to the transition to multipulsing is caused by the continuum amplification. This results from the lower gain saturation caused by the decrease in the pulse energy. The latter is induced by the growth of the pulse spectral loss due to the pulse shortening or its chirping. Since multiple-pulse generation originates from the continuum, the inter-pulse distances and phase differences are random.

The upper stability boundary corresponding to the transition to the stable or unstable multipulse generation comes from the growth of the perturbation bounded within the pulse profile. The continuum amplification plays the minor role in this case because the net gain for it is negative. As a result of the pulse energy growth accompanying the σ increase, the pulse splits and the pulse satellites appear. The inter-pulse distance, in this case, has a good repeatability and the phase difference change is very slow, so that there exists a set of attracting points, where an inter-pulse phase difference "stays" a longer time. This provides regular autocorrelation traces and spectral profiles.

Our analysis suggests the existence of the inter-pulse interaction producing their binding without the usual inter-soliton interaction through the oscillating tales. This interaction is caused by a balance of the saturable gain, the spectral and the saturable loss. As a result of this balance, there exists a preferred inter-pulse distance and a phase difference providing the minimal net-loss for the propagating pulses.

The revealed sources of multiple-pulse generation allow the formulation of the main methods to suppress multipulsing. These are reduction of the pump rate, decrease of the gain relaxation time, and increase of the loss modulation depth, the output loss, or the gain saturation. All these methods can shorten the pulse duration due to the extension of the single-pulse stability zone into the vicinity of zero GDD. However, this occurs at the cost of worse Kerr-lens mode locking self-starting ability or an increase of the σ parameter. The latter demands very thorough laser optimization because the high σ values in Kerr-lens mode-locked lasers are achieved only at the very edge of the resonator stability range.

The obtained numerical results are verified for the Cr^{2+}:ZnSe laser operating in the positive net-GDD region and for the Ti:sapphire laser operating in the regime of the chirp compensation. There is both qualitative and quantitative agreement between the theoretical and the experimental data. The presented analysis can be applied to the optimization of the lasers based on the various well known active media and to the estimation of the Kerr-lens mode locking stability of the new prospective active crystals.

References

[1] C. Spielmann, P. F. Curley, T. Brabec, and F.Ferenc Krausz, "Ultrabroad femtosecond lasers," *IEEE J. Quantum Electron.*, vol. 30, pp. 1100–1114, Apr. 1994.

[2] A. K. Komarov and K. P. Komarov, "Pulse splitting in a passive mode-locked laser," *Opt. Commun.*, vol. 183, pp. 265–270, 2000.

[3] V. P. Kalosha, M. Müller, J. Herrmann, and S. Gatz, "Spatiotemporal model of femtosecond pulse generation in Kerr-lens mode-locked solid-state lasers," *J. Opt. Soc. Amer. B*, vol. 15, pp. 535–550, 1998.

[4] M. J. Lederer, B. Luther-Davis, H. H. Tan, C. Jagadish, N. N. Akhmediev, and J. M. Soto-Crespo, "Multipulse operation of a Ti:sapphire laser mode locked by an ion-implanted semiconductor saturable-absorber mirror," *J. Opt. Soc. Amer. B*, vol. 16, pp. 895–904, 1999.

[5] J. N. Kutz, B. C. Collings, K. Bergman, and W. H. Knox, "Stabilized pulse spacing in soliton lasers due to gain depletion and recovery," *IEEE J. Quantum Electron.*, vol. 34, pp. 1749–1757, Sept. 1998.

[6] B. C. Collings, K. Bergman, and W. H. Knox, "True fundamental solitons in a passively mode-locked short-cavity Cr^{4+}:YAG laser," *Opt. Lett.*, vol. 22, pp. 1098–1100, 1997.

[7] B. A. Malomed, "Bound solitons in the nonlinear Schrödinger–Ginzburg–Landau equation," *Phys. Rev. A*, vol. 44, pp. 6954–6957, 1991.

[8] N. N. Akhmediev, A. Ankiewicz, and J. M. Soto-Crespo, "Multisoliton solutions of the complex Ginzburg–Landau equation," *Phys. Rev. Lett.*, vol. 79, pp. 4047–4051, 1997.

[9] V. V. Afanasjev and N. Akhmediev, "Soliton interaction in nonequilibrium dynamical systems," *Phys. Rev. E*, vol. 53, pp. 6471–6475, 1996.

[10] S. Namiki, E. P. Ippen, H. Haus, and C. X. Yu, "Energy equations for mode-locked lasers," *J. Opt. Soc. Amer. B*, vol. 14, pp. 2099–2111, 1997.

[11] V. L. Kalashnikov, I. G. Poloyko, V. P. Mikhailov, and D. von der Linde, "Regular, quasiperiodic and chaotic behavior in CW solid-state Kerr-lens mode-locked lasers," *J. Opt. Soc. Amer. B*, vol. 14, pp. 2691–2695, 1997.

[12] Q. Xing, L. Chai, W. Zhang, and C.-Y.Ch.-Yue Wang, "Regular, period-doubling, quasiperiodic, and chaotic behavior in a self-mode-locked Ti:sapphire laser," *Opt. Commun.*, vol. 162, pp. 71–74, 1999.

[13] V. L. Kalashnikov, I. G. Poloyko, N. I. Zhavoronkov, and V. P. Mikhailov, "Control of mode-locking efficiency in a Kerr-lens mode-locked Ti:sapphire laser," *J. Opt. Soc. Amer. B*, vol. 14, pp. 2705–2709, 1997.

[14] M. Lai, J. Nicholson, and W. Rudolph, "Multiple pulse operation of a femtosecond Ti:sapphire laser," *Opt. Commun.*, vol. 142, pp. 45–49, 1997.

[15] M. J. Bohn, R. J. Jones, and J.-C. Diels, "Mutual Kerr-lens mode-locking," *Opt. Commun.*, vol. 170, pp. 85–92, 1999.

[16] A. A. Hnilo and M. A. Larotonda, "Dynamics of the diode-pumped Kerr-lens mode-locked Nd:YAG laser," *J. Opt. Soc. Amer. B*, vol. 18, pp. 1451–1455, 2001.

[17] J. Jasapara, V. L. Kalashnikov, D. O. Krimer, I. G. Poloyko, M. Lenzner, and W. Rudolph, "Automodulations in CW Kerr-lens mode-locked solid-state lasers," *J. Opt. Soc. Amer. B*, vol. 17, pp. 319–326, 2000.

[18] V. L. Kalashnikov, D. O. Krimer, and I. G. Poloyko, "Soliton generation and picosecond collapse in solid-state lasers with semiconductor saturable absorber," *J. Opt. Soc. Amer. B*, vol. 17, pp. 519–523, 2000.

[19] C.-Y.Ch.-Yue Wang, W. Zhang, K. F. Lee, and K. M. Yoo, "Pulse splitting in a self-mode-locking Ti:sapphire laser," *Opt. Commun.*, vol. 137, pp. 89–92, 1997.

[20] H. Kitano and S. Kinoshita, "Stable multipulse generation from a self-mode-locked Ti:sapphire laser," *Opt. Commun.*, vol. 157, pp. 128–134, 1998.

[21] D. E. Spence and W. Sibbett, "Femtosecond pulse generation by a dispersion-compensated, coupled-cavity, mode-locked Ti:sapphire laser," *J. Opt. Soc. Amer. B*, vol. 8, pp. 2053–2060, 1991.

[22] I. T. Sorokina, E. Sorokin, E. Wintner, A. Cassanho, H. P. Jenssen, and R. Szipocs, "Sub-20 fs pulse generation from the mirror dispersion controlled Cr:LiSGaF and Cr:LiSAF lasers," *Appl. Phys. B*, vol. 65, pp. 245–253, 1997.

[23] H. Liu, J. Nees, and G. Mourou, "Doide-pumped Kerr-lens mode-locked Yb:KY(WO_4^2 laser," *Opt. Lett.*, vol. 26, pp. 1723–1725, 2001.

[24] J. Aus der Au, D. Kopf, F. Morier-Genoud, M. Moser, and U. Keller, "60-fs pulses from a doide-pumped Nd:glass laser," *Opt. Lett.*, vol. 22, pp. 307–309, 1997.

[25] B. C. Collings, K. Bergman, and W. H. Knox, "True fundamental solitons in a passively mode-locked short-cavity Cr^{4+}:YAG laser," *Opt. Lett.*, vol. 22, pp. 1098–1100, 1997.

[26] I. T. Sorokina, E. Sorokin, A. Di Lieto, M. Tonelli, P. H. Page, and K. I. Schaffers, "Active and passive mode-locking of Cr^{2+}:ZnSe laser," in *Trends in Optics and Photonics*, C. Marshall, Ed. Washington, DC: OSA, 2001, vol. 50, pp. 157–161.

[27] L. D. DeLoach, R. H. Page, G. D. Wilke, S. A. Payne, and W. P. Krupke, "Transition metal-doped Zinc chalcogenides: spectroscopy and laser demonstration of a new class of gain media," *IEEE J. Quantum Electron.*, vol. 32, pp. 885–895, June 1996.

[28] R. H. Page, K. I. Schaffers, L. D. DeLoach, G. D. Wilke, F. D. Patel, J. B. Tassano, S. A. Payne, W. F. Krupke, K.-T. Chen, and A. Burger, "Cr^{2+}-doped zinc chalcogenids as efficient widely tunable mid-infrared lasers," *IEEE J. Quantum Electron.*, vol. 33, pp. 609–619, 1997.

[29] R. H. Page, J. A. Skidmore, K. I. Schaffers, R. J. Beach, S. A. Payne, and W. P. Krupke, "Demonstrations of diode-pumped and grating-tuned ZnSe:Cr^{2+} lasers," in *Trends in Optics and Photonics*, C. R. Pollock and W. R. Bosenberg, Eds. Washington, DC: OSA, 1997, vol. 10, pp. 20–21.

[30] E. Sorokin, I. T. Sorokina, and R. H. Page, "Room-temperature CW diode-pumped Cr^{2+}:ZnSe laser," in *Trends in Optics and Photonics*, C. Marshall, Ed. Washington, DC: OSA, 2001, vol. 50, pp. 101–105.

[31] A. V. Podlipensky, V. G. Shcherbitsky, N. V. Kuleshov, V. I. Levchenko, V. N. Yakimovich, M. Mond, E. Heumann, G. Huber, H. Kretschmann, and S. Kück, "Efficient laser operation and continuous-wave diode-pumping of Cr^{2+}:ZnSe single crystals," *Appl. Phys. B.*, vol. 72, pp. 253–255, 2001.

[32] T. J. Carrig, G. J. Wagner, A. Sennaroglu, J. Y. Jeong, and C. R. Pollock, "Mode-locked Cr^{2+}:ZnSe laser," *Opt. Lett.*, vol. 25, pp. 168–170, 2000.

[33] G. Fibich and A. L. Gaeta, "Critical power for self-focusing in bulk media and and in hollow waveguides," *Opt. Lett.*, vol. 25, pp. 335–337, 2000.

[34] V. L. Kalashnikov, E. Sorokin, and I. T. Sorokina, "Mechanisms of spectral shift in ultrashort-pulse laser oscillators," *J. Opt. Soc. Amer. B*, vol. 18, pp. 1732–1741, 2001.

[35] V. L. Kalashnikov, V. P. Kalosha, V. P. Mikhailov, I. G. Poloyko, and M. I. Demchuk, "Self-mode locking of continuous-wave solid-state lasers by a nonlinear Kerr polarization modulator," *J. Opt. Soc. Amer. B*, vol. 10, pp. 1443–1446, 1993.

[36] S. A. Akhmanov, V. A. Vysloukh, and A. S. Chirkin, *Optics of Femtosecond Laser Pulses*. New York: Springer, 1992, ch. 2.

[37] J. P. Gordon, "Dispersive perturbations of solitons of the nonlinear Schrödinger equation," *J. Opt. Soc. Amer. B*, vol. 9, pp. 91–97, 1992.

[38] Q. Lin and I. Sorokina, "High-order dispersion effects in solitary mode-locked lasers: sideband generation," *Opt. Commun.*, vol. 153, pp. 285–288, 1998.

[39] H. A. Haus, J. G. Fujimoto, and E. P. Ippen, "Analytic theory of additive pulse and Kerr lens mode locking," *IEEE J. Quantum Electron.*, vol. 28, pp. 2086–2096, Oct. 1992.

[40] V. L. Kalashnikov, V. P. Kalosha, I. G. Poloyko, and V. P. Mikhailov, "Optimal resonators for self-mode locking of CW solid-state lasers," *J. Opt. Soc. Amer. B.*, vol. 14, pp. 964–968, 1997.

[41] F. X. Kärtner, I. D. Jung, and U. Keller, "Soliton mode-locking with a slow saturable absorber," *IEEE J. Select. Topics Quantum Electron.*, vol. 2, pp. 540–555, Sept. 1996.

[42] V. L. Kalashnikov, V. P. Kalosha, I. G. Poloyko, and V. P. Mikhailov, "Mode locking of CW solid-state lasers with a slow saturable absorber," *Opt. Spectrosc.*, vol. 81, pp. 794–799, 1996.

[43] J. M. Soto-Crespo, N. N. Akhmediev, and V. V. Afanasjev, "Stability of the pulselike solitons of the quintic complex Ginzburg-Landau equation," *J. Opt. Soc. Amer. B*, vol. 13, pp. 1439–1449, 1996.

[44] J. Herrmann and M. Müller, "Theory of nonlinear coupled-cavity mode locking," *J. Opt. Soc. Amer. B*, vol. 13, pp. 1542–1558, 1996.

[45] Mathematical ultrashort-pulse laser physics, V. L. Kalashnikov. (2002). [Online]. Available: http://xxx.lanl.gov/physics/0009056.

[46] J. P. Gordon, "Interaction forces among solitons in optical fibers," *Opt. Lett.*, vol. 8, pp. 596–598, 1983.

[47] G. Agrawal, *Nonlinear Fiber Optics*. San Diego, CA: Academic, 1989, p. 131.

[48] Y. Kodama and S. Wabnitz, "Reduction and suppression of soliton interactions by bandpass filters," *Opt. Lett.*, vol. 18, pp. 1311–1313, 1993.

[49] V. V. Afanasjev, "Interpretation of the effect of reduction of soliton interaction by bandwidth-limited amplification," *Opt. Lett.*, vol. 18, pp. 790–792, 1993.

[50] I. V. Barashenkov and E. V. Zemlyanaya, "Stable complexes of parametrically driven, damped nonlinear Schrödinger solitons," *Phys. Rev. Lett.*, vol. 83, pp. 2568–2571, 1999.

Vladimir L. Kalashnikov was born in Minsk, Belarus, in 1965. He received the diploma degree in physics in 1989 and the Ph.D. degree in laser physics in 1992 from Belorussian State University, Minsk, for theoretical work on mode-locked solid-state lasers.

He was with the Institute for Applied Physics Problems from 1989 to 1993, first as a Junior Researcher, then as Senior Researcher. During 1993–1996, he held a Scientific Secretary position at the International Laser Center, Belorussian Polytechnic Academy. In 1996, he was a Visiting Scientist at the Institute for Laser- and Plasmophysics, University of Essen, Germany. From 1996, he was a Head of the Laser Optics Laboratory, International Laser Center, Belarus, and an Associate Professor in the Instrument-Industry Department, Belorussian Polytechnic Academy. In 2001, he joined the Photonics Institute, Technical University of Vienna, Austria, as a Lise Meitner Fellow, supported by the Austrian National Science Found (FWF). His research interests include the nonlinear optics of femtosecond pulses, the dynamics of solid-state and fiber lasers, the computer algebra approaches to an analysis of nonlinear phenomena and cosmology. He is the author and co-author of more than 130 publications in scientific journals and proceedings of international conferences.

Evgeni Sorokin was born in Moscow, Russia, in 1962. He received the M.S. degree in physics and mathematics from the Moscow M. V. Lomonosov State University in 1986 and the Ph.D degree in technical physics from the Vienna University of Technology, Vienna, Austria, in 1994 for "Spectroscopy and laser properties of disordered crystals."

In 1986, he joined the research staff of the General Physics Institute of the Russian Academy of Sciences, working on high-temperature Raman spectroscopy of solids and melts, and while also teaching at the Moscow Physics and Technology Institute. He has been with the Quantum Electronics and Laser Technology Group, Vienna University of Technology, since 1992, and since 1999, he has been an Assistant Professor with the Photonics Institute of the same university. His current research interests include physics of diode-pumped tunable and ultrashort-pulsed lasers based on novel rare-earth- and transition-metal-doped crystals. He has authored and co-authored more than 130 publications, including over 50 journal articles, and holds one patent.

Dr. Sorokin is a member of the Optical Society of America.

Irina T. Sorokina was born in Moscow, Russia, in 1963. She received the M.S. degree in physics from the Moscow Lomonosov State University in 1986 and the Ph.D degree in laser physics from the General Physics Institute of the Russian Academy of Sciences (GPI), Moscow, in 1992. Her doctoral study was focused on the electron excitation energy transfer processes from Cr to Nd, Tm and Ho ions in scandium garnet crystals.

Since 1986, she has been a Research Staff Scientist of the GPI. In 1989, she spent a few months as a Visiting Scientist with the Quantum Electronics Department of the Vienna University of Technology (TU Wien), Vienna, Austria. She is currently with the same department of the TU Wien, where she was a Lise-Meitner Fellow of the Austrian National Science Fund (FWF) from 1992 to 1994. As a Hertha-Firnberg Assistant Professor, she leads a research program in infrared vibronic solid-state lasers at the Photonics Institute, TU Wien. Her current research is focused on the development and characterization of the novel broad-band crystalline lasers, femtosecond pulse generation, nonlinear optics and physics of interionic processes in laser crystals. She was Chair of an international laser symposium, and is an author and coauthor of more than 140 journal/conference publications (including about 50 journal articles), a patent holder, and a coeditor of a book.

Dr. Sorokina is a member of the Austrian Physical Society, the Optical Society of America, and the Austrian Association of Scientists Wissenschaftsforum. She was awarded a Hertha-Firnberg Prize of the Austrian Ministery of Sciences and the FWF in 1999.